Research in Astron. Astrophys. **2009** Vol. **9** No. **1**, 41 – 58
http://www.raa-journal.org *http://www.iop.org/journals/raa*

***R**esearch in*
***A**stronomy and*
***A**strophysics*

Alignment between galaxies and large-scale structure *

A. Faltenbacher[1,2], Cheng Li[1,2], Simon D. M. White[1], Yi-Peng Jing[2], Shu-De Mao[3] and Jie Wang[4]

[1] Max-Planck-Institute for Astrophysics, Karl-Schwarzschild-Str. 1, D-85741 Garching, Germany; *afaltenbacher@mpa-garching.mpg.de*
[2] MPA/SHAO Joint Center for Astrophysical Cosmology at Shanghai Astronomical Observatory, Shanghai 200030, China
[3] Jodrell Bank Centre for Astrophysics, Alan Turing Building, The University of Manchester, Manchester M13 9PL, UK
[4] Department of Physics, Institute of Computational Cosmology, University of Durham, Science Laboratories, South Road, Durham DH1 3LE, UK

Received 2008 November 12; accepted 2008 December 12

Abstract Based on the Sloan Digital Sky Survey DR6 (SDSS) and the Millennium Simulation (MS), we investigate the alignment between galaxies and large-scale structure. For this purpose, we develop two new statistical tools, namely the *alignment correlation function* and the $\cos(2\theta)$*-statistic*. The former is a two-dimensional extension of the traditional two-point correlation function and the latter is related to the ellipticity correlation function used for cosmic shear measurements. Both are based on the cross correlation between a sample of galaxies with orientations and a reference sample which represents the large-scale structure. We apply the new statistics to the SDSS galaxy catalog. The alignment correlation function reveals an overabundance of reference galaxies along the major axes of red, luminous ($L \gtrsim L_*$) galaxies out to projected separations of $60\,h^{-1}\mathrm{Mpc}$. The signal increases with central galaxy luminosity. No alignment signal is detected for blue galaxies. The $\cos(2\theta)$-statistic yields very similar results. Starting from a MS semi-analytic galaxy catalog, we assign an orientation to each red, luminous and central galaxy, based on that of the central region of the host halo (with size similar to that of the stellar galaxy). As an alternative, we use the orientation of the host halo itself. We find a mean projected misalignment between a halo and its central region of $\sim 25\,^\circ$. The misalignment decreases slightly with increasing luminosity of the central galaxy. Using the orientations and luminosities of the semi-analytic galaxies, we repeat our alignment analysis on mock surveys of the MS. Agreement with the SDSS results is good if the central orientations are used. Predictions using the halo orientations as proxies for central galaxy orientations overestimate the observed alignment by more than a factor of 2. Finally, the large volume of the MS allows us to generate a two-dimensional map of the alignment correlation function, which shows the reference galaxy distribution to be flattened parallel to the orientations of red luminous galaxies with axis ratios of ~ 0.5 and ~ 0.75 for halo and central orientations, respectively. These ratios are almost independent of scale out to $60\,h^{-1}\mathrm{Mpc}$.

Key words: dark matter halos: clustering — galaxies: large — scale structure of Universe — cosmology: theory — dark matter

∗ Supported by the National Natural Science Foundation of China.

1 INTRODUCTION

Recent large redshift surveys, like the 2dF Galaxy Redshift Survey (2dFGRS, Colless et al. 2001) and the Sloan Digital Sky Survey (SDSS, York et al. 2000), allow the cosmic large-scale density field to be traced with unprecedented accuracy. Different structures can reliably be classified as groups, filaments, walls and voids and match well with the patterns seen in N-body simulations. These structures induce large-scale tidal fields which in turn cause large-scale correlations in the orientations of massive dark matter halos (cf. Bond et al. 1996; Colberg et al. 1999; Altay et al. 2006) . However, the orientations of dark matter halos are difficult to observe. One needs either X-ray observations for a sufficient number of groups and clusters of galaxies or reliable galaxy-group catalogs derived from the redshift surveys. The former are expensive and the latter are prone to a number of systematic errors. Despite these difficulties, both approaches have been pursued. In most cases, alignment signals out to at least $20\,h^{-1}\mathrm{Mpc}$ have been found (Binggeli 1982; Ulmer et al. 1989; West 1989b; Plionis 1994; Chambers et al. 2000; Hashimoto et al. 2007). Instead of measuring the large-scale alignment based on groups and clusters of galaxies, we suggest here to directly use the orientations of luminous galaxies and we quantify their alignment relative to large-scale structure.

Galaxies are not oriented at random. Rather, they have been found to show various forms of spatial alignment: between neighboring clusters of galaxies (Binggeli 1982; West 1989a; Plionis 1994), between the brightest cluster galaxies (BCGs) and their parent clusters (Carter & Metcalfe 1980; Binggeli 1982; Struble 1990; Hashimoto et al. 2008), between the orientation of satellite galaxies and the orientation of the cluster (Dekel 1985; Plionis et al. 2003), and between the orientation of satellite galaxies and the orientation of the BCG (Struble 1990).

Observationally, these alignments are quantified either by the differential, $P(\theta)$, or cumulative, $P(\theta \leq \theta_{\mathrm{max}})$, probability distribution of the alignment angle θ, which is the angle between the major axis of a galaxy and the line connecting it to a neighboring galaxy. Also, the mean values of those distributions, $\langle\theta\rangle(r_p)$, have been studied as a function of projected separation r_p. With recent large redshift surveys, in particular the SDSS, it has become possible to determine the alignment using large and homogeneous samples. Studies based on these surveys have focused mainly on the alignment of galaxies in groups. They revealed that satellite galaxies are preferentially distributed along the major axis of the central galaxies (Brainerd 2005; Yang et al. 2006; Azzaro et al. 2007; Faltenbacher et al. 2007), and satellite galaxies tend to be preferentially oriented toward the central galaxy (Pereira & Kuhn 2005; Agustsson & Brainerd 2006; Faltenbacher et al. 2007). Donoso et al. (2006) analyzed a high-redshift sample ($0.4 < z < 0.5$) of luminous red galaxies (LRGs) extracted from the SDSS, and found a clear signal of alignment between LRG major axes and the distribution of galaxies within $1.5h^{-1}$Mpc, indicating that the alignment effects observed in the local Universe were already present at $z \sim 0.5$.

In this paper, we propose two new statistics to quantify the alignment between galaxies and the large-scale structure. The first one we call the *alignment two-point correlation function*, which is an extension of the traditional two-point correlation function. Basically, the correlation is measured as a function of pair separation and alignment angle. The second measure we call $\cos(2\theta)$*-statistic* and involves determining the mean cosine of twice the alignment angle for correlated pairs of given projected separation. We measure these statistics for SDSS galaxies as well as for semi-analytic galaxies within the Millennium simulation (MS) (Springel et al. 2005; De Lucia & Blaizot 2007), where the orientations of the semi-analytic galaxies are inferred from the orientation of their parent dark matter halos. The application of the new statistics reveals an alignment between red galaxies and large-scale structure out to $60\,h^{-1}\mathrm{Mpc}$.

The paper is organized as follows. In Section 2, we introduce the two statistics used here to quantify the alignment between galaxies and large-scale structure. The statistics are applied to the SDSS galaxy catalog in Section 3 and compared to the results derived from the semi-analytic galaxy catalog of the MS in Section 4. Finally, Section 5 gives a short summary.

2 METHODOLOGY

For the subsequent analysis, we introduce two new statistical measures to quantify the correlations between galaxy orientations and the cosmic density field. We call the first quantity the *alignment (two-point) correlation function*, $w_p(\theta_p, r_p)$, where θ_p is the angle between the major axis of a galaxy and the connecting line to another one and r_p is the projected separation between the two galaxies. This quantity is a two-dimensional extension of the traditional two-point projected correlation function. Paz et al. (2008) have used a related technique to analyze large-scale angular momentum alignments. The second quantity we refer to as the $\cos(2\theta)$*-statistic*. This statistic is closely related to similar quantities used in the context of cosmic shear surveys. We compute both statistics only in projected space, i.e. orientations and pair separations are two-dimensional vectors. We keep this restriction also in the second part of this analysis where we compare observational and numerical results.

2.1 Alignment Correlation Function

The two-point correlation function (2PCF) has long served as the primary way of quantifying the clustering properties of galaxies in redshift surveys (e.g. Peebles 1980). It is defined as a function of pair separation by

$$dP_{12} = \bar{n}^2[1 + \xi(\mathbf{r})]dV_1 dV_2, \tag{1}$$

where $\xi(\mathbf{r})$ is the 2PCF, $\bar{n}$ the mean number density of galaxies, and dV_1 and dV_2 are two infinitesimal volume elements centered at $\mathbf{x}_1$ and $\mathbf{x}_2$ with separation $\mathbf{r} = \mathbf{x}_2 - \mathbf{x}_1$. To be consistent with homogeneity and isotropy, ξ has been written as a function of the separation alone, that is, $\xi(r)$. If $\xi(r) \neq 0$, then galaxies are said to be clustered. As the fundamental second-order statistic of the density field, ξ is simple to compute and provides a full statistical description for a Gaussian random field (Bardeen et al. 1986). It can also be easily compared with the predictions of theoretical models (e.g. Aarseth et al. 1979; Davis et al. 1985). The amplitude of the correlation function on scales larger than a few Mpc provides a direct measure of the mass of the dark matter halos that host the galaxies through the halo mass-bias relation (e.g. Mo & White 1996; Jing et al. 1998).

In galaxy redshift surveys, the 2PCF is measured in redshift space and expressed either as a function of redshift-space separation s, giving rise to a 2PCF of $\xi(s)$, or as functions of separations perpendicular (r_p) and parallel (π) to the line of sight, giving rise to $\xi(r_p, \pi)$ with $s^2 = \pi^2 + r_p^2$. In many cases, the projected 2PCF, $w_p(r_p)$, is the more useful quantity, as it does not suffer from redshift-space distortions, and is thus directly related to the real-space correlation function $\xi(r)$. One can distinguish between two kinds of two-point correlation functions: *two-point auto-correlation functions* for which both members of a pair come from the same sample, and *two-point cross-correlation functions* (2PCCFs) for which the two members of a pair are from two different samples. In this paper, we focus on the latter. In addition, our analysis will be pursued in projected space, i.e. we focus on the projected 2PCCF $w_p(r_p)$, where r_p denotes the projected separation of a galaxy pair.

Given a sample of galaxies in question (Sample Q), a sample of reference galaxies (Sample R), and a random sample (Sample $\mathcal{R}$) that has the same selection function (i.e. distribution of redshifts and positions in the sky) as the reference sample, $\xi(r_p, \pi)$ between Q and R can be estimated by

$$\xi(r_p, \pi) = \frac{N_{\mathcal{R}}}{N_R} \frac{QR(r_p, \pi)}{Q\mathcal{R}(r_p, \pi)} - 1, \tag{2}$$

where N_R and $N_{\mathcal{R}}$ are the number of galaxies contained in the reference and random samples, with $N_{\mathcal{R}}/N_R = 10$ throughout this paper. $QR(r_p, \pi)$ and $Q\mathcal{R}(r_p, \pi)$ are the counts of cross pairs between the indicated samples for a given separation perpendicular, r_p, and parallel, π, to the line-of-sight. With the measurement of $\xi(r_p, \pi)$ in hand, one can then estimate the projected cross-correlation function $w_p(r_p)$ by integrating $\xi(r_p, \pi)$ along the π direction:

$$w_p(r_p) = \int_{-\pi_{\max}}^{+\pi_{\max}} \xi(r_p, \pi) d\pi = \sum_i \xi(r_p, \pi_i) \Delta\pi_i, \tag{3}$$

where $\pi_{\rm max}$ has to be sufficiently large to minimize the probability of erroneously excluding correlated pairs with line-of-sight separations larger than $\pi_{\rm max}$.

Now we extend the definition of the 2PCCFs, so that they will be able to quantify the spatial alignment of galaxies. For each pair of galaxies with one member from Sample Q (the main galaxy) and the other from Sample R (the reference galaxy), we consider θ_p, the angle between the major axis of the main galaxy and the line connecting the two galaxies projected onto the sky. We include this angle as a second property of the pair, in addition to the pair separation. In this case, the correlation function is not only a function of the projected separations, but also of θ_p. The estimator of Equation (4) is easily modified to account for the dependence on θ_p:

$$\xi(\theta_p, r_p, \pi) = \frac{N_{\mathcal{R}}}{N_R} \frac{QR(\theta_p, r_p, \pi)}{Q\mathcal{R}(\theta_p, r_p, \pi)} - 1, \tag{4}$$

$QR(\theta_p, r_p, \pi)$ and $Q\mathcal{R}(\theta_p, r_p, \pi)$ are the counts of cross pairs between the indicated samples for given θ_p, r_p and π. The projected correlation function is found by integration along the line-of-sight.

$$w_p(\theta_p, r_p) = \int_{-\pi_{\rm max}}^{+\pi_{\rm max}} \xi(\theta_p, r_p, \pi) d\pi = \sum_i \xi(\theta_p, r_p, \pi_i) \Delta\pi_i. \tag{5}$$

The traditional correlation function is just the average of the new correlation function over the full range of θ_p values. Taking symmetries into account, the value of the angle ranges from zero (along the major axis of the main galaxy) to 90 degrees (perpendicular to the major axis). Thus, higher amplitudes of the new correlation functions at small values of θ_p indicate that the reference galaxies are more likely to be aligned along the major axis of the main galaxies. In contrast, higher amplitudes at larger angles indicate that the reference galaxies are more likely to be located along the minor axis of the main galaxies. This new statistic can be used for quantifying the alignment of galaxies and we refer to it as the *alignment correlation function*.

On small scales ($\lesssim$ Mpc), this statistic can be used to confirm the alignment between central and satellite galaxies in groups and clusters, if Sample Q consists purely of central galaxies (cf. Carter & Metcalfe 1980; Binggeli 1982; Struble 1990). More interestingly, the new statistic allows us to extend the alignment study to very large scales without worrying about selection effects, which are taken into account by comparison with the random sample ($\mathcal{R}$). On large scales, this statistic can be used to quantify the alignment of the main galaxies (which may or may not be central galaxies) with respect to the large-scale structure of the Universe as probed by the large-scale distribution of the reference galaxies.

As the final remark of this section, we would like to mention that one can easily derive equivalent expressions for the alignment *auto*-correlation function – additionally, it is straightforward to extend the formalism to three dimensional problems.

2.2 $\cos(2\theta)$-Statistic

The $\cos(2\theta)$-statistic gives the average of $\cos(2\theta_p)$ for all correlated pairs at a given projected separation. It will be referred as $\langle\cos(2\theta_p)_{\rm cor}\rangle(r_p)$ where the index cor emphasizes that the average is based on correlated pairs only. Again, θ_p indicates the angle between the major axis of a main galaxy and the line connecting it with a reference galaxy. More precisely, using the alignment correlation function, $w_p(\theta_p, r_p)$, we define

$$\langle\cos(2\theta_p)_{\rm cor}\rangle(r_p) = \frac{\int_0^{\pi/2} \cos(2\theta_p) w_p(\theta_p, r_p) d\theta_p}{\int_0^{\pi/2} w_p(\theta_p, r_p) d\theta_p}\,. \tag{6}$$

This statistic is constrained to values between -1 and 1. Values above and below 0 indicate a preference for small ($< 45^\circ$) and large ($> 45^\circ$) angles, respectively. Values close to 0 are expected for isotropy. An

estimator for Equation (6) is given by

$$\langle \cos(2\theta_p)_{\rm cor} \rangle (r_p) = \frac{\sum_i \left(\frac{QR_\theta(r_p,\pi_i)}{Q\mathcal{R}(r_p,\pi_i)} \right) \Delta\pi_i}{\sum_i \left(\frac{QR(r_p,\pi_i)}{Q\mathcal{R}(r_p,\pi_i)} - 1 \right) \Delta\pi_i} \,, \tag{7}$$

where $QR_\theta(r_p, \pi_i)$ symbolizes the sum of $\cos(2\theta_p)$ for all cross pairs between main and reference samples (Q and R) within the given separation bins, r_p and π_i. As before, $QR(r_p, \pi_i)$ and $Q\mathcal{R}(r_p, \pi_i)$ denote the number of cross pairs between the indicated samples for r_p and π_i.

Related statistics are used in weak lensing studies where they are referred to as ellipticity correlations (e.g. Miralda-Escude 1991; Croft & Metzler 2000; Heavens et al. 2000). In particular, we want to point out the similarity to the intrinsic shear-density correlation function $w_{g+}(r_p)$ (Mandelbaum et al. 2006; Hirata et al. 2007), which measures the correlation between galaxy orientations and the large-scale density distribution. Leaving the ellipticity weighting and 'responsivity' correction aside, (cf. Eqs. (8) and (9) in Hirata et al. 2007) the following relation holds.

$$\tilde{w}_{g+} = w_p(r_p) \langle \cos(2\theta_p) \rangle_{\rm cor}(r_p), \tag{8}$$

where $\tilde{w}_{g+}$ indicates the unweighted version of w_{g+}. We do not weight by ellipticity since we here are solely interested in the spatial alignment between galaxies and the large-scale structure.

3 ALIGNMENT OF SDSS GALAXIES

In this section, we apply the two new statistics to the publicly available data from the Sloan Digital Sky Survey DR6. Before doing that, we describe some details about the survey and the galaxy sample construction. Also, the determination of the galaxy orientations is reviewed.

3.1 Galaxy Sample Construction

The observational data used in this paper are taken from the SDSS, which has been designed to obtain photometry of a quarter of the sky and spectra of nearly one million objects. Imaging is obtained in the *u, g, r, i, z* bands (Fukugita et al. 1996; Smith et al. 2002; Ivezić et al. 2004). The details of the survey strategy can be found in York et al. (2000) and an overview of the data pipelines and products is provided in the Early Data Release paper (Stoughton et al. 2002). The SDSS has had seven additional major data releases (Abazajian et al. 2003, 2004, 2005; Adelman-McCarthy et al. 2006, 2007, 2008).

The galaxy samples for this work are constructed from `Sample dr6` of the New York University Value Added Galaxy Catalog (NYU-VAGC), which is based on the SDSS DR6, publicly available at *http://sdss.physics.nyu.edu/vagc/*. A detailed description thereof can be found in Blanton et al. (2005). Our sample consists of 430164 galaxies that are identified as galaxies from the Main sample (note that r-band magnitude has been corrected for foreground extinction), and are in the ranges of $0.01 < z < 0.4$, $-23 < M_{0.1r} < -17$ and $14.5 < r < 17.6$. Here $M_{0.1r}$ is the r-band absolute magnitude corrected to its $z = 0.1$ value using the $K-$correction code of Blanton et al. (2003b) and the luminosity evolution model of Blanton et al. (2003a). We do not consider galaxies fainter than $M_{0.1r} = -17$, because the volume covered by such faint samples is very small and the results are subject to large errors as a result of cosmic variance (see for example fig. 6 of Li et al. 2006). The faint apparent magnitude limit of 17.6 is chosen to yield a uniform galaxy sample that is complete over the entire area of the survey. This sample will serve as the reference sample (Sample R) for computing cross-correlation functions, as well as the parent sample for selecting different subsamples (Q).

The large amount of data allows us to split the parent sample into various subsamples. Thus, we split all the galaxies into 4 subsamples according to their r-band absolute magnitudes, ranging from $M_{0.1r} = -23$ to $M_{0.1r} = -17$ with an interval of 1 magnitude. Furthermore, we classify each galaxy with $M_{0.1r} > -22$ as either "red" or "blue" according to its $g - r$ color. To this end, we follow Li et al. (2006) to fit the $g - r$ distribution at fixed luminosity with a bi-Gaussian profile and use the mean of

the two Gaussian centers as the color cut. In the highest luminosity bin, $-23 < M_{0.1r} < -22$, this color separation scheme is problematic, basically because the blue population is extremely sparse, thus we assign all galaxies within this magnitude bin to the red population (cf. Li et al. 2006, fig. 9). These subsamples will be cross-correlated with the full parent sample, i.e. the reference sample.

To compute the cross-correlation function between the main and reference samples, Q and R, one also needs to construct a random sample, $\mathcal{R}$, where galaxies with random coordinates are subject to the same selection effects as the reference sample. Since the reference sample is used as a tracer of the large-scale structure, only the galaxy positions instead of their orientations are of interest. Accordingly, orientations are not considered when constructing the random sample. A detailed account of the selection effects accompanies the NYU-VAGC release (Blanton et al. 2005) which is the basis of the construction of the random sample used here (cf. Li et al. 2006).

3.2 Determination of Galaxy Orientations

The orientation of galaxies is quantified by the position angle (PA) of the major axis of their r-band images, which is determined by the SDSS photometric pipeline called PHOTO (Lupton et al. 2001). PHOTO provides three quantities for the PA of each galaxy: $\mathrm{PA}_{\mathrm{deV}}$, $\mathrm{PA}_{\mathrm{exp}}$, and $\mathrm{PA}_{\mathrm{iso}}$. The first two come from fitting two models to the two-dimensional image of the galaxy in each band: a pure de Vaucouleurs profile and a pure exponential profile, while the last one is given by measuring the shape parameters (centroid, major and minor axes, PA, and average radius) of the 25 mag arcsec $^{-2}$ isophote. Details of the photometric pipeline can be found in Lupton et al. (2001) and Stoughton et al. (2002). In this paper, we use the isophotal PA, $\mathrm{PA}_{\mathrm{iso}}$. However, we found no significant variation in the alignment signals when adopting the alternative definitions for the PAs.

To quantify the intrinsic scatter of the alignment signal, we randomly shuffle the PAs among the galaxies in the main sample and redo the alignment analysis. Since the shuffled orientations are not correlated with the large-scale structure, one expects no systematic alignment signal. The 1σ variance of 10 randomly shuffled samples can then be used to infer the intrinsic scatter.

3.3 Alignment Correlation Function

We now compute the alignment correlation function, $w_p(\theta_p, r_p)$, based on Equation (5) with $\pi_{\max} = 40\,h^{-1}\mathrm{Mpc}$. We probe projected separations up to $60\,h^{-1}\mathrm{Mpc}$ within three angular bins. A less coarse angular binning is prohibited by Poisson noise at large separations.

3.3.1 Alignment for red galaxies

The first row of the upper panel of Figure 1 shows the alignment correlation function for red galaxies in various magnitude bins. The red, green and blue solid lines display the results for the different angular bins, $0^\circ - 30^\circ$, $30^\circ - 60^\circ$ and $60^\circ - 90^\circ$, respectively. The low angle bin, $0^\circ - 30^\circ$, quantifies the correlation function along the orientation of the main galaxies. The $60^\circ - 90^\circ$ bin contains information about the reference galaxy abundance perpendicular to the orientation of the main galaxies. The long dashed black line represents the traditional correlation function and is a weighted average of the three bins.

The second row of the upper panel of Figure 1 shows the ratio of the alignment correlation function to the traditional one. The color code is the same as used in the row above. The shaded regions indicate the 1σ variance between 10 random samples in which the orientations are shuffled at random among the galaxies. A signal well outside the shaded region is a significant detection of alignment or anti-alignment depending on whether the signal lies above or below one.

The alignment correlation functions (colored lines) for red galaxies in the lowest luminosity bin ($-20 < M_{0.1r} < -19$) can hardly be distinguished from the traditional correlation function (dashed black line). However, the corresponding ratio, $w_p(\theta_p, r_p)/w_p(r_p)$, shows a weak but systematic trend to anisotropy at scales larger than $\sim 10\,h^{-1}\mathrm{Mpc}$. At these separations, the reference galaxies are preferentially located along the major axes of the main galaxies. Along the minor axes, the reference galaxies

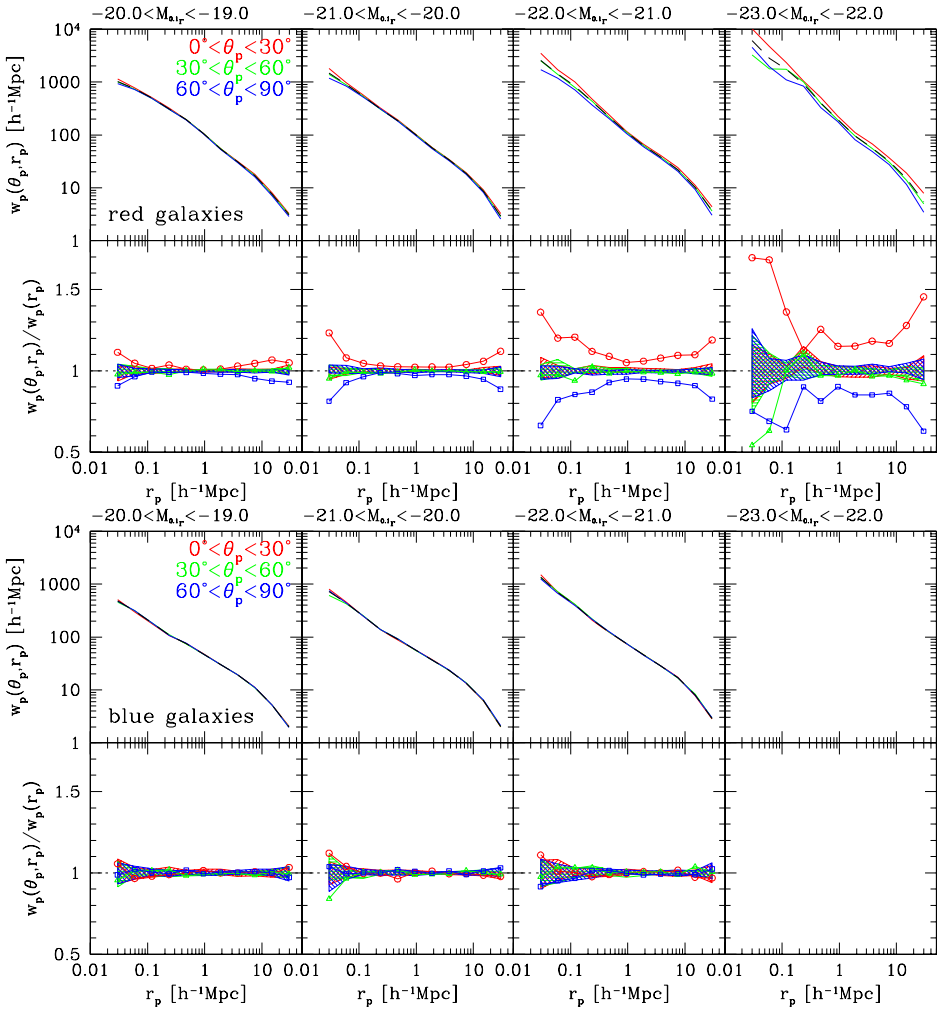

Fig. 1 *Upper panels in each set:* Solid lines display the projected SDSS alignment correlation function, $w_p(\theta_p, r_p)$, between our reference sample and red (upper set) and blue (lower set) main galaxies in different intervals of r-band absolute magnitude. The colors correspond to three ranges in θ_p as indicated. The dashed black line shows the conditional correlation function averaged over angle. *Lower panels in each set:* Ratio between the angle dependent correlation functions and their mean. The color code is the same as used in the upper panels. The shaded regions plotted in red, green and blue colors indicate the $1-\sigma$ variance based on 10 samples in which the position angles are shuffled at random among the galaxies. By definition (Sect. 3.1), there are no blue galaxies in the brightest luminosity bin, so these panels are kept void.

are correspondingly under-abundant. This feature becomes more pronounced in higher luminosity bins. For galaxies brighter than $M_{0.1r} = -20$, a significant overabundance of reference galaxies is visible along the major axis. The signal reaches from $10\,h^{-1}\mathrm{kpc}$ out to $60\,h^{-1}\mathrm{Mpc}$ which corresponds to the entire range probed here.

These plots indicate that the orientations of red galaxies are connected to the large-scale structure in which they are embedded. Any realistic galaxy formation model should be able to reproduce this interlacing between dimensions spanning ~ 3 orders of magnitude.

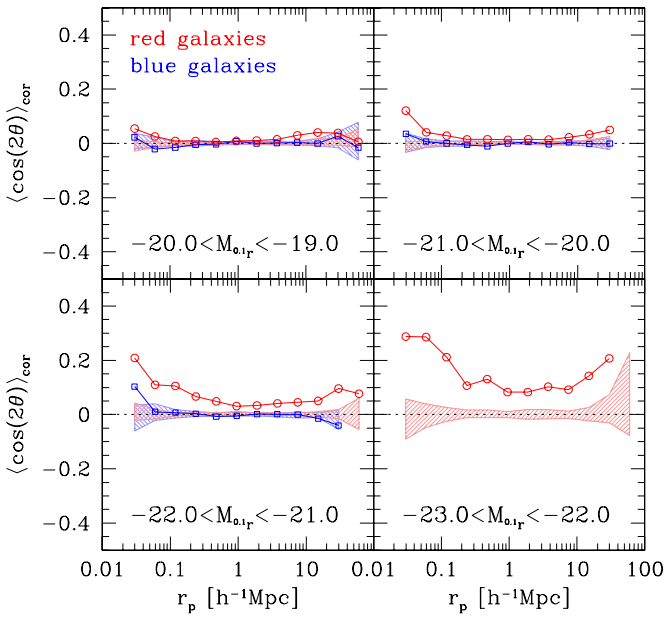

Fig. 2 $\cos(2\theta_p)$ statistic for SDSS data. The results for red and blue main galaxies are displayed by red and blue lines. The galaxies are subdivided into four r-band absolute magnitude bins as indicated. The shaded regions in red and blue show the 1σ variance between 10 random samples in which the position angles are shuffled at random among the main galaxies. The reference sample is the same for all these measurements and comprises all galaxies with r-band absolute magnitudes in $-23 < M_{0.1_r} < -17$. No results are shown for blue galaxies in the highest luminosity since, by definition, they are red galaxies.

3.3.2 Alignment for blue galaxies

The lower panels of Figure 1 display the corresponding results for blue galaxies. Otherwise, the analysis is carried out in exactly the same manner as for the red galaxies. The panel for the highest magnitude bin, $-23 < M_{0.1_r} < -22$, is left void because, by definition, there are no blue galaxies with these luminosities (see Sect. 3.1). In the lower three magnitude bins, we do not find any indication for alignment between the galaxies and the reference galaxy distribution. The differences seen between red and blue galaxies suggest that the orientations of red and blue galaxies are determined by distinct physical processes.

3.4 $\cos(2\theta)$-Statistic

In this section, we compute the $\cos(2\theta)$ statistic based on the same subdivision of the parent SDSS sample by color and r-band absolute magnitude as used above for the alignment correlation function. In the second step, we focus on the alignment signal for group central galaxies. This is to facilitate a comparison with simulation results discussed in the second part of this paper.

3.4.1 Color and luminosity dependence

Figure 2 displays the $\cos(2\theta_p)$-statistic as discussed in Section 2.2. The results for red and blue galaxies are displayed by red and blue lines. The shaded regions show the 1σ variance between the 10 random samples. The signal for the red galaxies shows a strong dependence on luminosity. There is basically no signal for red galaxies in the lowest luminosity bin. For r-band absolute magnitudes, ranging from

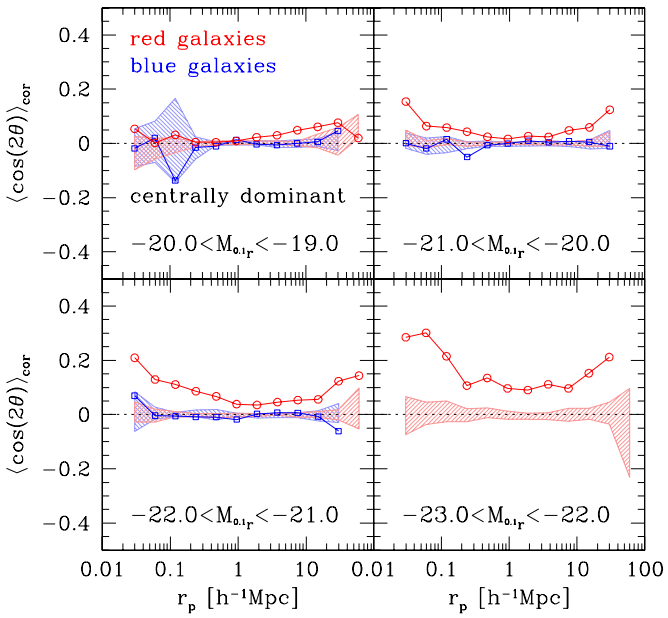

Fig. 3 $\cos(2\theta_p)$ statistic for SDSS central galaxies. See the text for our definition of 'central'. Results for red and blue galaxies are displayed by red and blue lines. All symbols are the same as used in Fig. 2.

$M_{0.1r} = -20$ to $M_{0.1r} = -23$, the signal systematically lies above the shaded region, indicating that it cannot be explained by the intrinsic scatter inherent in the data. The signal is significant on all scales probed ($\leq 60\,h^{-1}\mathrm{Mpc}$) and becomes more pronounced with increasing luminosity. Blue galaxies do not show any indication for alignment with the reference galaxy distribution. Figure 2 suggests that red galaxies with $L \gtrsim L_*$ tend to be aligned with large-scale structure out to at least $60\,h^{-1}\mathrm{Mpc}$. This result is very similar to that from the alignment correlation function discussed in Section 3.3. It supports the picture of a physically distinct origin for the orientations of red and blue galaxies.

3.4.2 Alignment of group central galaxies

Alignment between clusters of galaxies has been detected out to large scales $\sim 100\,h^{-1}\mathrm{Mpc}$ (e.g., Binggeli 1982; Plionis 1994; Hashimoto et al. 2007). In addition, there exists strong evidence that the orientations of central galaxies are aligned with the orientations of their parent groups or clusters. Now the question arises whether an exclusion of non-central galaxies may enhance the alignment signal measured before. To this end, we redo the above analysis excluding *non-central* galaxies. This approach also facilitates a subsequent comparison with N-body results, since there, only the orientations of central galaxies are available (see Sect. 4.4).

Central galaxies are found in the following way. For each main galaxy, we use its r-band absolute magnitude to calculate a halo mass, according to the relation between central galaxy luminosity and halo mass as given by Yang et al. (2005a). We then estimate a 'virial' radius using the model of Eke et al. (2001). We find all the companions around the galaxy within this radius and a line of sight velocity separation of $\pm 3000\,\mathrm{km\,s^{-1}}$ and compare the luminosity of the galaxy to that of the companions. If the galaxy is brighter than any of its companions and it is not inside the virial radius of a farther, brighter galaxy, it is classified as a 'central' galaxy. Otherwise, it is a 'non-central' galaxy. This method will inevitably mis-judge a certain fraction of galaxies to be non-central due to the appearance of more luminous interlopers (cf. Yang et al. 2005b). However, it should be sufficient to estimate the signal

for central galaxies. This can then be compared to the signal for the complete sample as well as to simulations.

Figure 3 displays the alignment signals based on central galaxies only. As before, we do not find any alignment signal for blue galaxies. The upper two luminosity bins show only marginal differences when compared to the complete sample. This can be explained by the fact that most bright galaxies are central. For the lower two luminosity bins, the alignment signal increases by a few per cent which indicates a certain reduction of the alignment signal for the complete sample which includes non-central galaxies (Fig. 2). We come to the conclusion that the alignment signal is not strongly enhanced by the exclusion of non-central galaxies which is due in part to the fact that luminous galaxies usually are central.

4 COMPARISON TO THE ALIGNMENT OF MS GALAXIES

In the second part of this study, we apply our new analysis tools (alignment correlation function and $\cos(2\theta)$-statistic) to semi-analytic galaxies in the MS. Orientations have to be assigned to the model galaxies and we investigate different approaches, comparing the resulting alignment signals with the observed ones. Since we did not detect any alignment signal for blue galaxies, we restrict our orientation assignment to red model galaxies. This restriction may also be justified by a slightly different kind of reasoning. Namely, red luminous galaxies are predominantly elliptical galaxies. Those are thought to form via merging of proto-galaxies which is basically a collisionless process. Thus N-body simulations may be able to recover some characteristic features of red galaxies, in particular, their orientation. Blue galaxies, on the other hand, are mainly spiral galaxies with their properties heavily dependent on baryonic, i.e. collisional, physics. Thus, their properties may be only poorly recovered by N-body simulations. This picture may change at high redshifts. At that time, also, the orientation of many blue galaxies could be a product of gas-rich mergers.

In the following two paragraphs, we list some details of the MS and describe how we estimate orientations for the model galaxies. Subsequently, we redo the analysis already carried out on SDSS galaxy samples and we compare the results.

4.1 The Simulation and the Galaxy Sample

The Millennium Simulation (Springel 2005) adopted concordance values for the parameters of a flat Λ cold dark matter (ΛCDM) cosmological model, $\Omega_{\rm dm} = 0.205$ and $\Omega_{\rm b} = 0.045$ for the current densities in CDM and baryons, $h = 0.73$ for the present dimensionless value of the Hubble constant, $\sigma_8 = 0.9$ for the rms linear mass fluctuation in a sphere of radius $8\,h^{-1}{\rm Mpc}$ extrapolated to $z = 0$, and $n = 1$ for the slope of the primordial fluctuation spectrum. The simulation followed 2160^3 dark matter particles from $z = 127$ to the present day within a cubic region $500\,h^{-1}{\rm Mpc}$ on a side resulting in individual particle masses of $8.6 \times 10^8\,h^{-1}{\rm M}_\odot$. The gravitational force had a Plummer-equivalent comoving softening of $5\,h^{-1}{\rm kpc}$. The Tree-PM N-body code GADGET2 (Springel et al. 2005) was used to carry out the simulation and the full data were stored 64 times spaced approximately equally in the logarithm of the expansion factor. This information makes it possible to construct trees that store detailed assembly histories for each dark matter halo present at $z = 0$.

The halos are found by a two-step procedure. In the first step, all collapsed halos with at least 20 particles are identified using a friends-of-friends (FoF) group-finder with linking parameter b = 0.2. These objects will be referred to as *FoF-halos*. Then, post-processing with the substructure algorithm SUBFIND (Springel et al. 2001) subdivides each FoF-halo into a set of self-bound *sub-halos*. Here we only consider the *main sub-halo* which is the sub-halo with the most massive progenitor among all sub-halos belonging to the same FoF-halo. We refer to this sub-halo as the parent sub-halo associated with the central galaxy.

Based on the assembly histories, individual halos are populated with semi-analytic galaxies for which many 'observable' quantities are generated. For a detailed description of the construction of the semi-analytic galaxy catalog, we refer the reader to Croton et al. (2006) and De Lucia & Blaizot (2007). Here, we use the DeLucia2006a_SDSS2MASS catalog (*http://www.g-vo.org/MyMillennium2/*)

Table 1 Particle number statistics for host halos.

M_r	$[-20,-19]$	$[-21,-20]$	$[-22,-21]$	$[-23,-22]$
$N_{\rm halo}$	16027	98618	167513	53065
$\langle N_{\rm sub}\rangle$	489	1672	4707	18662
$\langle N_{\rm cen}\rangle$	31	83	164	278

which provides synthetic magnitudes through SDSS filters; alternatively to classify the model galaxies as well as to tag their parent sub-halos. The use of semi-analytic galaxies facilitates comparison to the observations and is also an elegant way to characterize the assembly history of the host halo by a few numbers.

Our standard reference sample comprises a random subset (1103640 galaxies) of all semi-analytic galaxies with r-band absolute magnitudes of $-23 \leq M_r \leq -17$ (in total 11027979 galaxies) at $z = 0$. This standard reference sample is used for all the subsequent analysis based on MS galaxies. The parent galaxy sample comprises all red, central galaxies within the same magnitude range as the reference galaxies ($-23 \leq M_r \leq -17$). A galaxy is red if $g - r \geq 0.7$, where g and r are synthetic magnitudes in the corresponding SDSS bands. A galaxy is central if it is the dominant galaxy in a given FoF-halo. Expressed in the MS terminology, it is the (only) type 0 galaxy within this FoF-halo. This definition comes close to the selection we have employed to identify central galaxies in the observational analysis above. In analogy to the SDSS sample, the MS galaxies are split into four r-band magnitude bins with equal intervals of one magnitude. Each model galaxy is associated with a dark matter halo which will be used to determine the orientation of the galaxy. For the four magnitude bins that Table 1 lists: the number of halos ($N_{\rm halo}$); the average number of particles belonging to these halos, $\langle N_{\rm sub}\rangle$; and the average number of particles belonging to the central part of the halos, $\langle N_{\rm cen}\rangle$. The determination of the number of central particles is related to the computation of the central orientations and will be discussed below. We conclude this paragraph by emphasizing that orientations are only determined for red, central galaxies, because only for those galaxies do we expect a tight correlation between the orientations of galaxy and halo.

4.2 The Orientations of Semi-Analytic Galaxies

As a proxy for the major axis of the central galaxy, we adopt the major axis of the projected moment of inertia tensor of the parent sub-halo (cf. Agustsson & Brainerd 2006; Kang et al. 2007; Faltenbacher et al. 2008; Knebe et al. 2008; Okumura et al. 2008). Since real galaxies are seen in projection, we project the dark matter distribution before diagonalizing the moment of inertia tensor. We determine the orientations of each central galaxy in two alternative ways. We use the dark matter distribution of the parent sub-halo, (i.e. the main sub-halo of the FoF-halo) or we only use its central part to approximate the orientation of the central galaxy. The former is done to compare the results to earlier work while the latter better mimics the true physical circumstance (cf. Faltenbacher et al. 2008; Knebe et al. 2008). We will refer to the former as *halo orientation* and the latter as *central* or *galaxy orientation*. The central orientation is determined in an iterative way. We begin by computing a number of central particles $N_{\rm cen}$ using the following formula

$$N_{\rm cen} = \begin{cases} 37 & \times N_{\rm sub}^{0.2} \quad \text{for } N_{\rm sub} \geq 4900, \\ 0.225 & \times N_{\rm sub}^{0.8} \quad \text{for } N_{\rm sub} < 4900, \end{cases} \tag{9}$$

where $N_{\rm sub}$ is the number of particles within the parent sub-halo. This formula is a two-power-law approximation to the observed relation between the luminosity of a central galaxy and its parent halo mass (e.g. Cooray & Milosavljević 2005). It reflects the assumption that the distribution of a galaxy's stellar component can be represented by the central matter distribution of its simulated dark matter halo. The

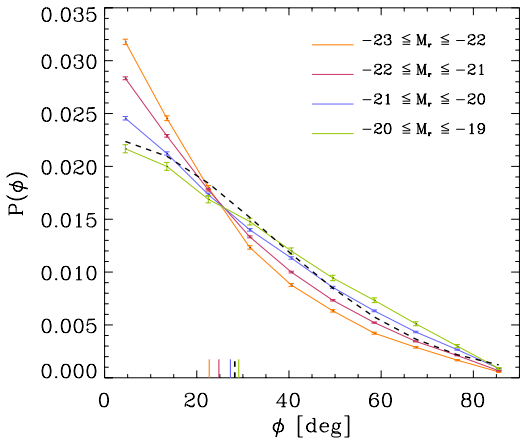

Fig. 4 Probability distribution of the misalignment angle between halo and central (galaxy) orientations for a series of magnitude bins as indicated. Errors represent Poisson uncertainties. The small vertical lines on the bottom axis denote the mean values of the distributions. The dashed line displays the result of Okumura et al. (2008) and its mean which we show as a black dashed mark on the bottom axis.

mass representing the galaxy then has to follow the observed scaling laws. Now, let $r_{\rm init}$ be the radius which encloses the $N_{\rm cen}$. In a first iteration step, the moment of inertia is computed within the $r_{\rm init}$. The resulting axis ratios are used to cut out a central ellipsoidal where the length of the intermediate axis is fixed to $r_{\rm init}$. Based on this new subset of particles, the moment of inertia is computed anew. The iteration is continued until the central orientation converges. Fixing the intermediate axis results in approximately unchanging particle numbers within consecutive ellipsoids. Up to this point, the computations were done in three dimensions. In a last step, all particles within the final ellipsoid are projected onto the plane of the sky. The inertia tensor of this 2-D distribution determines the central orientation.

In Figure 4, the difference between halo and central (galaxy) orientations are illustrated by the probability distribution function (PDF) of the misalignment angle between them. The mean values of the misalignment for each magnitude bin are indicated by the little vertical marks on the bottom axis. As indicated in Table 1, on average there are only 31 particles used to determine the central orientations within the lowest luminosity bin. Thus, Poisson noise adds an additional misalignment component which contributes to the flattening of the PDF at small angles. In fact, calculating the misalignment using central volumes twice as large as given by Equation (9) substantially reduces the flattening in the lowest luminosity bin. However, since we aim to probe the volume actually occupied by the stellar component of the galaxies, we adhere to Equation (9) keeping in mind that the central orientations for the low luminosity galaxies are poorly resolved. Such effects are less important for the higher luminosity bins. The two highest luminosity bins use 160 and 270 particles on average which should result in a robust determination of the orientations (cf. Jing 2002). For comparison, we also display the Gaussian PDF suggested by Okumura et al. (2008), who found a mean misalignment angle of $\sim 25\,^\circ$ between the halo and the galaxy orientation. Comparing the orientations of central galaxies and their host halos, a similar misalignment has been found by Agustsson & Brainerd (2006) and Kang et al. (2007). Somewhat lower values are quoted in Wang et al. (2008). The misalignment weakens slightly with increasing luminosity of the central galaxy, though this may be due to the resolution effects discussed above.

4.3 Alignment Correlation Function

With these orientations and the model magnitudes, the alignment correlation function can be computed for the galaxies in the MS. We will adopt the same luminosity bins used for our analysis of the SDSS

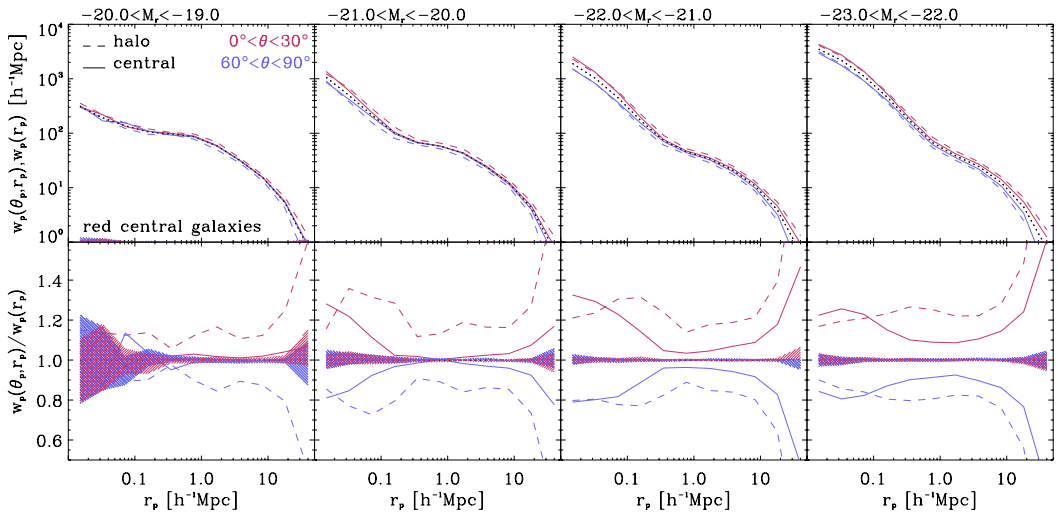

Fig. 5 *Upper panels:* Projected MS alignment correlation function, $w_p(\theta_p, r_p)$, for red central galaxies in different intervals of r-band absolute magnitude using the standard reference sample. The colors correspond to the sectors as indicated. The solid and dashed lines are based on central and halo orientations. The dotted line represents the traditional projected two-point cross-correlation function, $w_p(r_p)$. *Lower panels:* Ratio between the alignment and traditional correlation functions. The color code is the same as used above. Red and blue shaded regions indicate the $1-\sigma$ variance based on 10 samples in which the central orientations are shuffled at random among the galaxies.

data, simplifying the comparison between observations and simulations. For the computation of the alignment angle, we apply the distant observer approximation. To that end, the z-direction in the simulation is chosen to be parallel to the line of sight. To mimic the observational approach, the maximum projected separation of pairs along the line of sight is $\pi_{\rm max} = 40\,h^{-1}{\rm Mpc}$.

Figure 5 shows the alignment correlation function for four luminosity bins which can be compared to the upper panel in Figure 1. Also, the luminosity range of the reference sample is chosen to be the same as in our observational analysis. At this point, we would like to emphasize that the MS main sample only includes central galaxies. This causes the pronounced bend at a few hundred $h^{-1}{\rm kpc}$ corresponding roughly to virial radii of the host halos. The general behavior, however, is very similar to that seen in Figure 1. The correlation function is enhanced along the major axes of the red galaxies ($0^\circ < \theta_p < 30^\circ$) and reduced perpendicular to them. For galaxies brighter than $M_r \leq -20$, a systematic alignment/anti-alignment signal is seen over the entire separation range probed (out to $60\,h^{-1}{\rm Mpc}$). Also, the strength of the alignment effect increases with the luminosity of the galaxies.

In addition, we find that, except for small (intra-halo) scales, the alignment signal based on the halo orientations is more pronounced than that based on the central (galaxy) orientations. This can be explained by the misalignment between halo and central orientations discussed in Section 4.2. A comparison with the upper panel of Figure 1 reveals that the alignment based on halo orientations overestimates the observational signal whereas that based on the central orientations reproduces the amplitudes obtained for SDSS galaxies quite well.

So far, we have restricted the computation of the alignment correlation to 3 angular bins, a relatively coarse segmentation. This facilitates the direct comparison with the SDSS results, derived above, where a less coarse binning would result in excessive Poisson noise. However, the MS provides much better statistics, making possible the computation of a 2D alignment correlation map as displayed in Figure 6. This shows the alignment cross-correlation between a sample consisting of red ($g - r \geq 0.7$), central

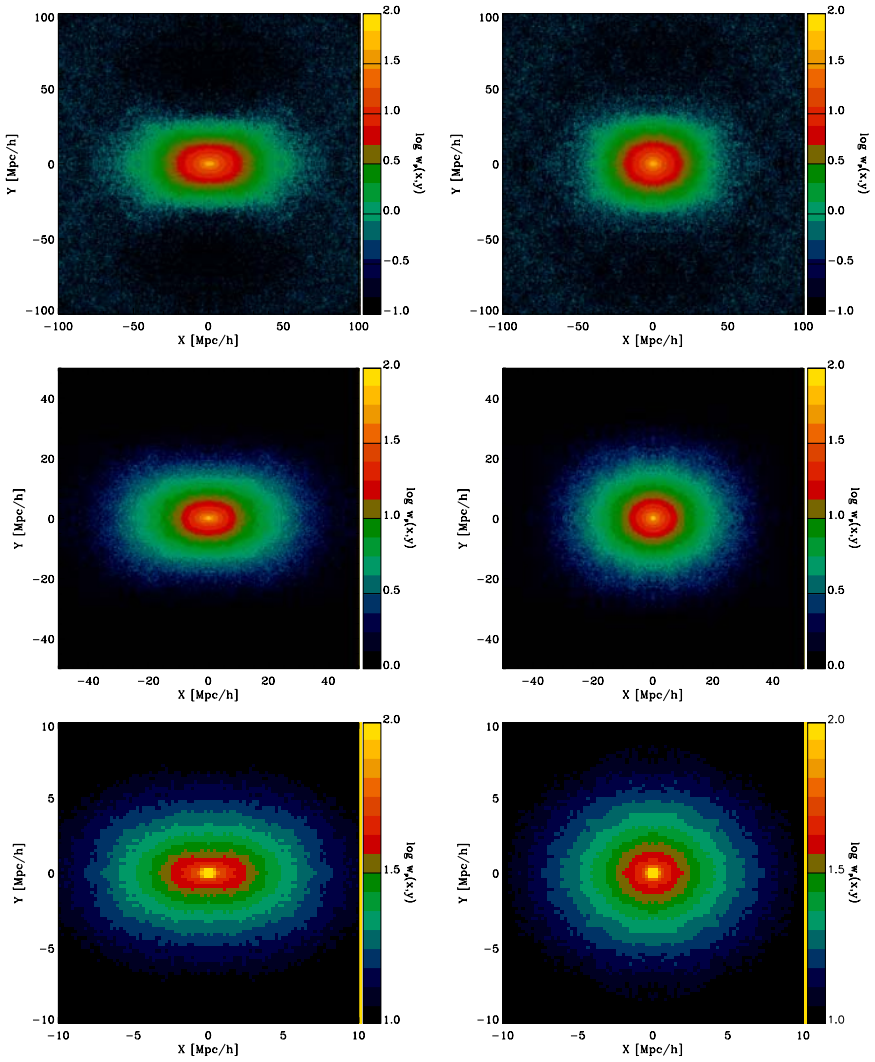

Fig. 6 2D alignment correlation function based on the DeLucia2006a_SDSS2MASS semi-analytic galaxy catalog for the MS. The main sample consists of red, central galaxies with absolute r-band magnitudes between -21 and -22. The orientations of the galaxies are aligned with the x-axis. Left and right panels display results based on halo and central orientations. Panels from top to bottom show the same distribution for different scales. The color code indicates the correlation amplitude, its range changes from top to bottom. Pixels with values below and above the indicated range are displayed black and yellow, respectively. The ratios of minor to major axes at $\log w_p(x, y) = 1.5$, 1 and 0.5 are 0.57, 0.61 and 0.42 for the halo and 0.75, 0.80, 0.75 for the central orientations.

galaxies with r-band luminosities between –21 and –22 and our standard reference sample. The left and right panels are based on halo and central orientations, respectively. The panels in a column display consecutive blowups of the same map. The correlation amplitude can be read off using the adjacent color bars. Note, the range changes from top to bottom. The ratios of minor to major axes for $\log w_p(x, y) = 1.5$, 1 and 0.5 are 0.57, 0.61 and 0.42 for the halo orientations and 0.75, 0.80, 0.75 for the central orientations. In agreement with the results above, the alignment correlation based on halo orientations

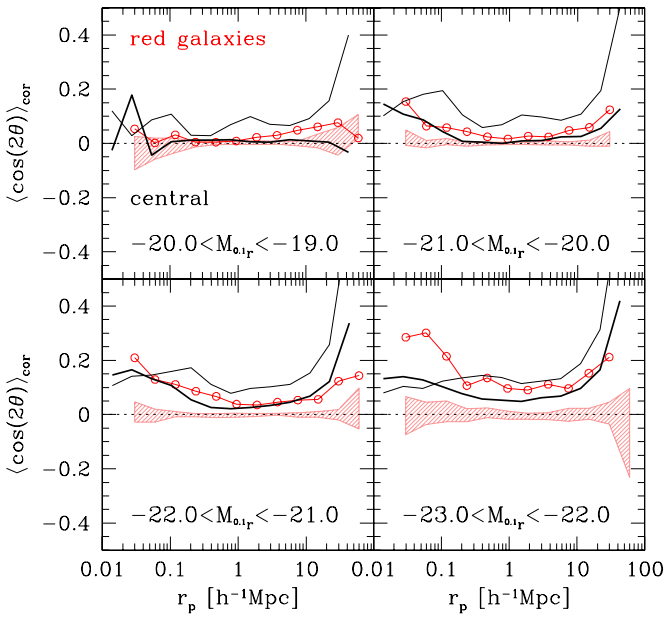

Fig. 7 Comparison of the $\cos(2\theta)$ signal for red SDSS galaxies and semi-analytic galaxies. The red lines and symbols are copied from Fig. 3. The black lines display the corresponding results derived from semi-analytic galaxy catalogs. Thin lines are based on the halo-orientations and thick lines represent results based model central-orientations.

is more anisotropic. It is striking that the flattening of the counts is almost constant over the range of scales we can measure.

The main conclusion to be drawn from Figures 5 and 6 is that the halos of red luminous galaxies are aligned with the surrounding galaxy distribution out to at least $60\,h^{-1}\mathrm{Mpc}$. If the orientations of the galaxies are approximated by the orientation of the halos as a whole, the alignment signal is strong. The misalignment between the halo and central region, as discussed in Section 4.2, causes a weakening of the correlation. The detection of the alignment between red galaxies and the large-scale structure provides a tool to test predictions for the alignment of galaxies with their halos.

4.4 $\cos(2\theta)$-Statistic

To facilitate the comparison of observed and modeled $\cos(2\theta)$-statistics we follow the observational approach discussed in Section 3.3, i.e we use the equivalent luminosity and color cuts. Again the analysis is carried out in projected space where the z-axis is chosen to lie parallel to the line-of-sight and the distant observer approximation is applied. The maximum line-of-sight separation between correlated pairs is restricted to $40\,h^{-1}\mathrm{Mpc}$. Only the signal based on red ($g-r \geq 0.7$), central galaxies is compared to the corresponding SDSS results. The standard MS reference sample is used.

In Figure 7 the results for central, red SDSS galaxies are copied from Figure 3, including the shaded region reflecting the intrinsic scatter in the observational data. The black lines display the corresponding signals derived from the MS. Thick lines represent the results based on central orientations, whereas thin lines are based on halo orientations. In the lowest luminosity bin, the halo orientations result in a substantial alignment signal whereas the signal based on the central orientations and the SDSS data are in agreement with no detected alignment signal. For the next two luminosity bins, the signal based on central orientations agrees well with the SDSS data. The mismatch for the largest separation bin may be associated with the zero-crossing of the correlation function, because the response of the $\cos(2\theta)$-

statistic is very sensitive near this point. In the highest luminosity bin, there appears a disagreement between the MS signal based on central orientations for separations $\leq 5\,h^{-1}\mathrm{Mpc}$ and the SDSS measurements. The agreement is better with the MS results based on the halo as a whole. On larger scales $5\,h^{-1}\mathrm{Mpc} \lesssim r_p \lesssim 60\,h^{-1}\mathrm{Mpc}$, again, there is good agreement with the signal based on central orientations whereas that based on overall halo orientations is an overestimate by 50–100 per cent.

We are led to the following conclusions: 1) the alignment signal depends on the magnitude of the central galaxy and/or the mass of the host halo. 2) The alignment signal based on the orientation of the halo exceeds the observed signal, in most cases, whereas the central orientations generally result in good agreement between observations and simulations. 3) The alignment for red central galaxies with $M_{0.1r} < -20$ persists to the largest scales probed ($\sim 60\,h^{-1}\mathrm{Mpc}$).

5 SUMMARY

In the first part of this study, we use the SDSS DR6 galaxy catalog to quantify the alignment between galaxies and the large-scale structure. We develop two new statistics, namely the *alignment correlation function* and the $\cos(2\theta)$*-statistic*. The former is a two-dimensional extension of the traditional two-point correlation function taking into account the orientations of the main galaxies. The latter is related to the ellipticity correlation function used to analyze cosmic shear observations. In both cases, we represent the large-scale structure by a reference galaxy sample with absolute r-band magnitudes between -17 and -23.

The alignment correlation function is defined on the 2D plane of the sky. In our SDSS analysis, we use a polar coordinate system and probe the correlation function along the galaxy major axes focusing on the $0^\circ < \theta_p < 30^\circ$ sector, where θ_p is the angle between the major axis and the connecting line to a reference galaxy. The abundance of reference galaxies perpendicular to the major axes is represented by the counts within the $60^\circ < \theta_p < 90^\circ$ sector. The main results revealed by the alignment correlation function are: 1) The major axes of red galaxies with $M_{0.1r} < -20$ are significantly aligned with large-scale structure; 2) The signal is visible out to $60\,h^{-1}\mathrm{Mpc}$ (the range probed here); 3) Independent of luminosity, blue galaxies are not aligned with large-scale structure.

The $\cos(2\theta)$-statistic also probes the anisotropy of the reference galaxies around main galaxies and is related to the galaxy — intrinsic shear correlation function as discussed in Mandelbaum et al. (2006) and Hirata et al. (2007). In contrast to the alignment correlation function, it does not require angular binning. It also reveals significant alignment between red luminous galaxies and large-scale structure out to $60\,h^{-1}\mathrm{Mpc}$, but no alignment is detected for blue galaxies. The restriction to central galaxies results in a slight enhancement of the alignment signal for red galaxies, in particular, at lower luminosities and at large separations. However, the differences are small, indicating little reduction of the signal by satellite galaxies which may have orientations altered by the local tidal field (cf. Pereira & Kuhn 2005).

The second part of this study is based on a Millennium Simulation semi-analytic galaxy catalog where we have assigned an orientation to each red, luminous and central galaxy based on the orientation of the mass distribution of the inner halo. As an alternative identification of the orientation of the central galaxy, we also used the orientation of the host halo itself.

The mean projected misalignment angle between a halo as a whole and its central (galaxy) region is $\sim 25^\circ$. This misalignment decreases slightly with increasing luminosity of the central galaxy and/or its host halo mass. This behavior is particularly notable, since the relative size of the central region (used to determine the central orientation) decreases with halo mass (cf., Eq. (9)).

Based on the orientations and the luminosities of the semi-analytic red galaxies, we compute the alignment correlation function in the same manner as for the SDSS galaxy catalog. We find that the alignment signal based on the halo orientations overestimates that found for SDSS. With the central orientation, however, quite good agreement between the modeled galaxy sample and the observations has been achieved. In other words, a misalignment between halo and central orientations is crucial for matching the observed amplitude of the alignment signal. Our approach for computing the major axis of the central elliptical galaxy based on the central dark matter distribution is physically motivated and

results in the right amount of misalignment. However, any other process which leads to equal misalignment will be in agreement with our measurements as well.

The large data volume of the MS allows us to generate a two-dimensional map of the alignment correlation function $w_p(x, y)$, i.e. we can adopt a very fine two dimensional binning and still get a reasonable number of pair-counts for each bin. The maps based on halo orientation show a substantially flattened galaxy distribution around red main galaxies out to at least $60\,h^{-1}\mathrm{Mpc}$. Using central orientations, the flattening is reduced. In particular, we have shown a map based on red main galaxies with r-band magnitudes between -22 and -21 using the standard reference sample. There, the ratios of the minor to major axes at $\log w_p(x, y) = 1.5$, 1 and 0.5 are 0.57, 0.61 and 0.42 for halo orientations and 0.75, 0.80, 0.75 for central orientations. It is interesting that the flattening is almost independent of scale all the way from $1\,h^{-1}\mathrm{Mpc}$ to $60\,h^{-1}\mathrm{Mpc}$.

Acknowledgements We would like to thank the referee for valuable comments, which helped to improve the paper. AF and CL are supported by the Joint Postdoctoral Program in Astrophysical Cosmology of Max Planck Institute for Astrophysics and Shanghai Astronomical Observatory. AF acknowledges support from the European Science Foundation program 'Computational Astrophysics and Cosmology' and the Jodrell Bank Visitor Grant. YPJ is supported by NSFC (Nos. 10533030, 10821302, 10878001), by the Knowledge Innovation Program of CAS (No. KJCX2-YW-T05), and by 973 Program (No. 2007CB815402). SM acknowledges the Humboldt Foundation for travel support.

Funding for the SDSS and SDSS-II has been provided by the Alfred P. Sloan Foundation, the Participating Institutions, the National Science Foundation, the U.S. Department of Energy, the National Aeronautics and Space Administration, the Japanese Monbukagakusho, the Max Planck Society, and the Higher Education Funding Council for England. The SDSS Web Site is *http://www.sdss.org/*.

The SDSS is managed by the Astrophysical Research Consortium for the Participating Institutions. The Participating Institutions are the American Museum of Natural History, Astrophysical Institute Potsdam, University of Basel, University of Cambridge, Case Western Reserve University, University of Chicago, Drexel University, Fermilab, the Institute for Advanced Study, the Japan Participation Group, Johns Hopkins University, the Joint Institute for Nuclear Astrophysics, the Kavli Institute for Particle Astrophysics and Cosmology, the Korean Scientist Group, the Chinese Academy of Sciences (LAMOST), Los Alamos National Laboratory, the Max-Planck-Institute for Astronomy (MPIA), the Max-Planck-Institute for Astrophysics (MPA), New Mexico State University, Ohio State University, University of Pittsburgh, University of Portsmouth, Princeton University, the United States Naval Observatory, and the University of Washington.

References

Aarseth, S. J., Turner, E. L., & Gott, III, J. R. 1979, ApJ, 228, 664
Abazajian, K., Adelman-McCarthy, J. K., Agüeros, M. A., et al. 2004, AJ, 128, 502
Abazajian, K., Adelman-McCarthy, J. K., Agüeros, M. A., et al. 2005, AJ, 129, 1755
Abazajian, K., Adelman-McCarthy, J. K., Agüeros, M. A., et al. 2003, AJ, 126, 2081
Adelman-McCarthy, J. K., Agüeros, M. A., Allam, S. S., et al. 2008, ApJS, 175, 297
Adelman-McCarthy, J. K., Agüeros, M. A., Allam, S. S., et al. 2007, ApJS, 172, 634
Adelman-McCarthy, J. K., Agüeros, M. A., Allam, S. S., et al. 2006, ApJS, 162, 38
Agustsson, I. & Brainerd, T. G. 2006, ApJ, 650, 550
Altay, G., Colberg, J. M., & Croft, R. A. C. 2006, MNRAS, 370, 1422
Azzaro, M., Patiri, S. G., Prada, F., & Zentner, A. R. 2007, MNRAS, 376, L43
Bardeen, J. M., Bond, J. R., Kaiser, N., & Szalay, A. S. 1986, ApJ, 304, 15
Binggeli, B. 1982, A&A, 107, 338
Blanton, M. R., Brinkmann, J., Csabai, I., et al. 2003a, AJ, 125, 2348
Blanton, M. R., Lin, H., Lupton, R. H., et al. 2003b, AJ, 125, 2276
Blanton, M. R., Schlegel, D. J., Strauss, M. A., et al. 2005, AJ, 129, 2562
Bond, J. R., Kofman, L., & Pogosyan, D. 1996, Nature, 380, 603

Brainerd, T. G. 2005, ApJ, 628, L101
Carter, D. & Metcalfe, N. 1980, MNRAS, 191, 325
Chambers, S. W., Melott, A. L., & Miller, C. J. 2000, ApJ, 544, 104
Colberg, J. M., White, S. D. M., Jenkins, A., & Pearce, F. R. 1999, MNRAS, 308, 593
Colless, M., Dalton, G., Maddox, S., et al. 2001, MNRAS, 328, 1039
Cooray, A., & Milosavljević, M. 2005, ApJ, 627, L85
Croft, R. A. C., & Metzler, C. A. 2000, ApJ, 545, 561
Croton, D. J., Springel, V., White, S. D. M., et al. 2006, MNRAS, 365, 11
Davis, M., Efstathiou, G., Frenk, C. S., & White, S. D. M. 1985, ApJ, 292, 371
De Lucia, G. & Blaizot, J. 2007, MNRAS, 375, 2
Dekel, A. 1985, ApJ, 298, 461
Donoso, E., O'Mill, A., & Lambas, D. G. 2006, MNRAS, 369, 479
Eke, V. R., Navarro, J. F., & Steinmetz, M. 2001, ApJ, 554, 114
Faltenbacher, A., Jing, Y. P., Li, C., et al. 2008, ApJ, 675, 146
Faltenbacher, A., Li, C., Mao, S., et al. 2007, ApJ, 662, L71
Fukugita, M., Ichikawa, T., Gunn, J. E., et al. 1996, AJ, 111, 1748
Hashimoto, Y., Henry, J. P., & Boehringer, H. 2008, MNRAS, 390, 1562
Hashimoto, Y., Henry, J. P., & Böhringer, H. 2007, MNRAS, 380, 835
Heavens, A., Refregier, A., & Heymans, C. 2000, MNRAS, 319, 649
Hirata, C. M., Mandelbaum, R., Ishak, M., et al. 2007, MNRAS, 381, 1197
Ivezić, Ž., Lupton, R. H., Schlegel, D., et al. 2004, Astronomische Nachrichten, 325, 583
Jing, Y. P. 2002, MNRAS, 335, L89
Jing, Y. P., Mo, H. J., & Boerner, G. 1998, ApJ, 494, 1
Kang, X., van den Bosch, F. C., Yang, X., et al. 2007, MNRAS, 378, 1531
Knebe, A., Yahagi, H., Kase, H., Lewis, G., & Gibson, B. K. 2008, MNRAS, 388, L34
Li, C., Kauffmann, G., Jing, Y. P., et al. 2006, MNRAS, 368, 21
Lupton, R., Gunn, J. E., Ivezić, Z., Knapp, G. R., & Kent, S. 2001, in Astronomical Data Analysis Software and Systems X, ed. F. R. Harnden, Jr., F. A. Primini, & H. Payne, 238, 269
Mandelbaum, R., Seljak, U., Cool, R. J., et al. 2006, MNRAS, 372, 758
Miralda-Escude, J. 1991, ApJ, 380, 1
Mo, H. J., & White, S. D. M. 1996, MNRAS, 282, 347
Okumura, T., Jing, Y. P., & Li, C. 2008, ArXiv e-prints
Paz, D., Stasyszyn, F., & Padilla, N. 2008, ArXiv e-prints
Peebles, P. J. E. 1980, The large-scale structure of the universe (Research supported by the National Science Foundation. Princeton, N.J., Princeton University Press, 1980, 435)
Pereira, M. J. & Kuhn, J. R. 2005, ApJ, 627, L21
Plionis, M. 1994, ApJS, 95, 401
Plionis, M., Benoist, C., Maurogordato, S., Ferrari, C., & Basilakos, S. 2003, ApJ, 594, 144
Smith, J. A., Tucker, D. L., Kent, S., et al. 2002, AJ, 123, 2121
Springel, V. 2005, MNRAS, 364, 1105
Springel, V., White, S. D. M., Jenkins, A., et al. 2005, Nature, 435, 629
Springel, V., White, S. D. M., Tormen, G., & Kauffmann, G. 2001, MNRAS, 328, 726
Stoughton, C., Lupton, R. H., Bernardi, M., et al. 2002, AJ, 123, 485
Struble, M. F. 1990, AJ, 99, 743
Ulmer, M. P., McMillan, S. L. W., & Kowalski, M. P. 1989, ApJ, 338, 711
Wang, Y., Yang, X., Mo, H. J., et al. 2008, MNRAS, 385, 1511
West, M. J. 1989a, ApJ, 344, 535
West, M. J. 1989b, ApJ, 347, 610
Yang, X., Mo, H. J., Jing, Y. P., & van den Bosch, F. C. 2005a, MNRAS, 358, 217
Yang, X., Mo, H. J., van den Bosch, F. C., & Jing, Y. P. 2005b, MNRAS, 356, 1293
Yang, X., van den Bosch, F. C., Mo, H. J., et al. 2006, MNRAS, 369, 1293
York, D. G., Adelman, J., Anderson, Jr., J. E., et al. 2000, AJ, 120, 1579